HEALTH AND MEDICINE

Robust differentiation of human pluripotent stem cells into endothelial cells via temporal modulation of ETV2 with modified mRNA

Kai Wang[1,2], Ruei-Zeng Lin[1,2], Xuechong Hong[1,2], Alex H. Ng[3,4], Chin Nien Lee[1,2], Joseph Neumeyer[1], Gang Wang[5], Xi Wang[6], Minglin Ma[6], William T. Pu[5,7], George M. Church[3,8], Juan M. Melero-Martin[1,2,7]*

Human induced pluripotent stem cell (h-iPSC)–derived endothelial cells (h-iECs) have become a valuable tool in regenerative medicine. However, current differentiation protocols remain inefficient and lack reliability. Here, we describe a method for rapid, consistent, and highly efficient generation of h-iECs. The protocol entails the delivery of modified mRNA encoding the transcription factor *ETV2* at the intermediate mesodermal stage of differentiation. This approach reproducibly differentiated 13 diverse h-iPSC lines into h-iECs with exceedingly high efficiency. In contrast, standard differentiation methods that relied on endogenous *ETV2* were inefficient and notably inconsistent. Our h-iECs were functionally competent in many respects, including the ability to form perfused vascular networks in vivo. Timely activation of *ETV2* was critical, and bypassing the mesodermal stage produced putative h-iECs with reduced expansion potential and inability to form functional vessels. Our protocol has broad applications and could reliably provide an unlimited number of h-iECs for vascular therapies.

INTRODUCTION

Endothelial cells (ECs) are implicated in the pathogenesis of numerous diseases particularly because of their ability to modulate the activity of various stem cells during tissue homeostasis and regeneration (*1*, *2*). Consequently, deriving competent ECs is central to many efforts in regenerative medicine. The advent of human induced pluripotent stem cells (h-iPSCs) created an exciting and noninvasive opportunity to obtain patient-specific ECs. However, differentiating h-iPSCs into ECs (here referred to as h-iECs) with high efficiency, consistently, and in high abundance remains a challenge (*3*).

Current differentiation protocols are inspired by vascular development and rely on sequentially transitioning h-iPSCs through two distinct stages (referred to as stages 1 and 2 or S1-S2) (*4*). During S1, h-iPSCs differentiate into intermediate mesodermal progenitor cells (h-MPCs), a process regulated by Wnt and Nodal signaling pathways. In S2, h-MPCs acquire endothelial specification principally via vascular endothelial growth factor (VEGF) signaling (*4*). Existing protocols, however, are far from optimal. Limitations stem from the inherent complexity associated with developmental processes. First, directing h-MPCs to solely differentiate into h-iECs is not trivial. Recent reports estimate that with the canonical S1-S2 approach, less than 10% of the differentiated cells may actually be bona fide h-iECs (*3*). In addition, achieving consistent differentiation in different h-iPSC lines continues to be a challenge (*5*). This dependency on cellular origin makes the clinical translation of h-iECs problematic.

The transcription factor E26 transformation-specific variant 2 (*ETV2*) plays a nonredundant and indispensable role in vascular cell development (*6*–*9*). Expression of ETV2 is only required transiently. Recent studies have proposed reprogramming somatic cells using transducible vectors encoding *ETV2* (*10*–*13*). Nevertheless, the efficiency of direct reprogramming somatic cells [e.g., fibroblasts (FB)] into ECs remains exceedingly low, and achieving proper conversion into ECs would likely require exposure to ETV2 activity over a long period of time. Alternatively, a few studies have recently proposed directly inducing *ETV2* expression on h-iPSCs to induce EC differentiation (*14*–*16*). However, to date, methods have relied on early activation of *ETV2* in the h-iPSCs, thus bypassing transition through an intermediate mesodermal stage. Also, the functional competence of the resulting h-iECs remains somewhat unclear.

Here, we sought to develop a protocol that enables more consistent and highly efficient differentiation of h-iPSCs into h-iECs. We identified that a critical source of inconsistency resides in the inefficient activation of ETV2 during S2. To circumvent this constraint, we made use of chemically modified mRNA (modRNA), a technology that, in recent years, has improved the stability of synthetic RNA allowing its transfer into cells (and subsequent protein expression) in vitro and in vivo (*17*). We developed a synthetic modRNA to uniformly activate *ETV2* expression in h-MPCs, independently of the presence of exogenous VEGF. As a result, conversion of h-MPCs into h-iECs occurred rapidly and robustly. We reproducibly differentiated 13 different h-iPSC clonal lines into h-iECs with high efficiency (>90%). Moreover, we demonstrated that these h-iECs were phenotypically and functionally competent in many respects, including their ability to form perfused vascular networks in vivo.

RESULTS

Rapid and highly efficient differentiation of h-iPSCs into h-iECs

We developed a two-dimensional, feeder-free, and chemically defined protocol that relies on a timely transition of h-iPSCs through two distinct stages, each lasting 48 hours. First is the conversion of

[1]Department of Cardiac Surgery, Boston Children's Hospital, Boston, MA 02115, USA. [2]Department of Surgery, Harvard Medical School, Boston, MA 02115, USA. [3]Department of Genetics, Harvard Medical School, Boston, MA 02115, USA. [4]Department of Systems Biology, Harvard Medical School, Boston, MA 02115, USA. [5]Department of Cardiology, Boston Children's Hospital, Boston, MA 02115, USA. [6]Department of Biological and Environmental Engineering, Cornell University, Ithaca, NY 14853, USA. [7]Harvard Stem Cell Institute, Cambridge, MA 02138, USA. [8]Wyss Institute for Biologically Inspired Engineering, Harvard University, Cambridge, MA 02138, USA.
*Corresponding author. Email: juan.meleromartin@childrens.harvard.edu

h-iPSCs into h-MPCs. This step is similar to that in the standard S1-S2 differentiation protocol and thus is mediated by the activation of Wnt and Nodal signaling pathways using the glycogen synthase kinase 3 inhibitor CHIR99021 (Fig. 1A). Second, we converted the h-MPCs into h-iECs. This step is substantially different from the S1-S2 protocol, which relies on activation of endogenous *ETV2* via VEGF signaling. In contrast, our protocol used chemically modRNA to deliver exogenous *ETV2* to h-MPCs via either electroporation or lipofection (Fig. 1A).

Our customized two-step protocol (here referred to as S1-modETV2) rapidly and uniformly converted h-MPCs into h-iECs. Forty-eight hours after transfection of h-MPCs with modRNA(*ETV2*), ~95% of the cells were endothelial [VE-Cadherin$^+$/CD31$^+$ cells; Fig. 1B; see fig. S1 (A and B) for controls accounting for electroporation with no modRNA and with modRNA(GFP)]. In contrast, conversion during the standard S2 step (no modRNA) was slower and notably less efficient, with less than 30% VE-Cadherin$^+$/CD31$^+$ cells at the same time point (Fig. 1B). Conversion efficiency was dependent on the

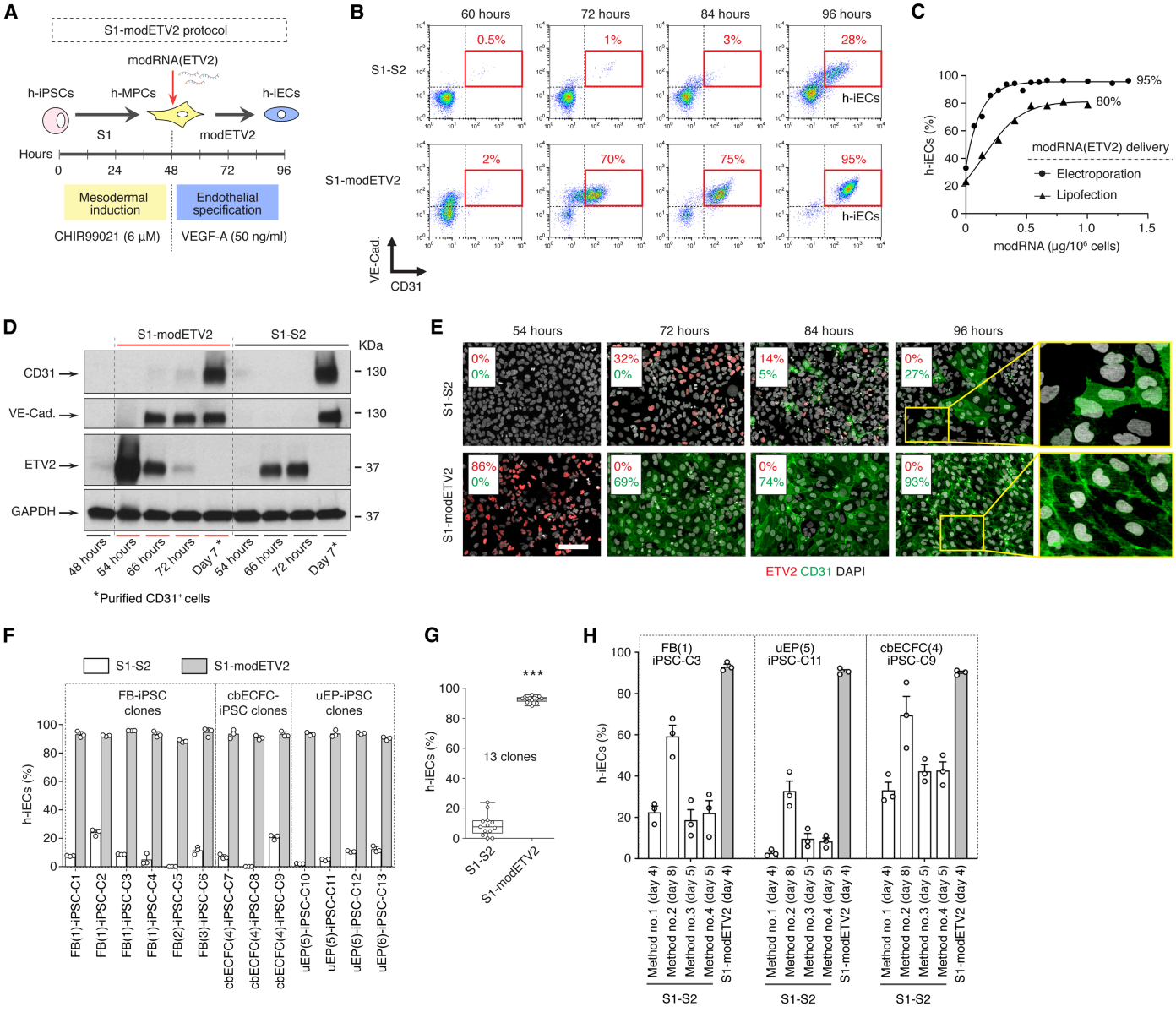

Fig. 1. Robust endothelial differentiation of h-iPSCs. (**A**) Schematic of two-stage EC differentiation protocol. Stage 1, conversion of h-iPSCs into h-MPCs. Stage 2, differentiation of h-MPCs into h-iECs via modRNA(ETV2). (**B**) Time course conversion efficiency of h-iPSCs into VE-Cadherin$^+$/CD31$^+$ h-iECs by flow cytometry ($n = 3$). (**C**) Effect of modRNA concentration on h-iPSC–to–h-iEC conversion at 96 hours. Analysis for both electroporation- and lipofection-based delivery of modRNA. (**D**) Western blot analysis of ETV2, CD31, and VE-Cadherin expression during EC differentiation. Lane 1 corresponds to cells at day 2 of the S1. GAPDH, glyceraldehyde-3-phosphate dehydrogenase. (**E**) Time course immunofluorescence staining for ETV2 and CD31 in S1-S2 and S1-modETV2 protocols (insets: mean %; $n = 3$). Nuclei stained by 4′,6-diamidino-2-phenylindole (DAPI). Scale bar, 100 μm. (**F**) Flow cytometry analysis of differentiation efficiency at 96 hours in 13 h-iPSC clones generated from dermal FBs, umbilical cbECFCs, and uEPs. (**G**) Differences in differentiation efficiency between S1-S2 and S1-modETV2 protocols for all 13 h-iPSC clones. Data correspond to percentage of CD31$^+$ cells by flow cytometry. (**H**) Differences in differentiation efficiency between four alternative S1-S2 methodologies and the S1-modETV2 protocol for three independent h-iPSC clones. Bars represent means ± SD; ***$P < 0.001$.

amount of modRNA(ETV2) used. Titration analysis revealed that above 0.5 μg of modRNA(ETV2) per 10^6 h-iPSCs, the percentage of h-iECs at 96 hours was consistently ~95% (using electroporation) and ~75% (lipofection) (Fig. 1C and fig. S1, C and D). Notably, the differentiation efficiency at 96 hours with the S1-modETV2 method was independent of the presence or absence of exogenous VEGF [fig. S1F; 93.74% efficiency with VEGF-A (50 ng/ml) from 48 to 96 hours and 94.08% without VEGF-A; $n = 4$].

Transfection with modRNA(ETV2) enabled rapid, transient, and uniform expression of ETV2, in contrast to delayed and sparse expression with the S1-S2 method (Fig. 1, D and E). Broad expression of ETV2, in turn, resulted in uniform CD31 expression by 96 hours (Fig. 1E). During the S1-S2 protocol, the presence of nonendothelial VE-Cadherin-/$SM22^+$ cells was prominent at 96 hours (fig. S1E). However, the occurrence of VE-Cadherin-/$SM22^+$ cells was significantly reduced in our S1-modETV2 protocol (<3%), suggesting a more effective avoidance of alternative nonendothelial differentiation pathways (fig. S1E).

Differentiation reproducibility with clonal h-iPSC lines from various cellular origins

Current S1-S2 differentiation protocols lack consistency between different h-iPSC lines. To address this limitation, we generated multiple human clonal h-iPSC lines from three distinct cellular origins corresponding to subcutaneous dermal FBs, umbilical cord blood-derived endothelial colony-forming cells (cbECFCs), and urine-derived epithelial cells (uEPs) (fig. S2A). All h-iPSCs were generated with a nonintegrating episomal approach and validated by expression of pluripotent transcription factors OCT4, NANOG, and SOX2 and capacity to form teratomas in immunodeficient mice (fig. S2, B and C).

We generated 13 clones (referred to as C1 to C13) to collectively represent variations due to different individual donors, cellular origins, and clone selection (fig. S2). All clones were subjected to both S1-S2 and S1-modETV2 differentiation protocols. As expected, the S1-S2 protocol produced a wide variation in efficiency, with h-iECs ranging from <1 to ~24% (Fig. 1, G and H). In addition, there were noticeable inconsistencies between clones from similar cellular origins but different donors (e.g., C2 versus C5 and C10 versus C13) and even between genetically identical clones derived from the same h-iPSC line (e.g., C2 versus C4, C8 versus C9, and C10 versus C12) (Fig. 1G). In contrast, differentiation under the S1-modETV2 protocol produced significantly higher efficiencies and eliminated inconsistencies between clones. In all 13 clones, the percentage of $CD31^+$ h-iECs at 96 hours ranged between 88 and 96% irrespective of the donor and cellular origin from which the h-iPSC clones were derived, and there were no statistical differences in efficiency (Fig. 1, G and H). Thus, the S1-modETV2 method was highly consistent in terms of differentiation efficiency across different clones.

To further corroborate these findings, we examined three additional S1-S2 methodologies corresponding to protocols described by Harding *et al.* (*18*) (method no. 2; duration, 8 days), Sahara *et al.* (*19*) (method no. 3; 5 days), and Patsch *et al.* (*4*) (method no. 4; 5 days). These methods were compared to our S1-S2 method (referred to as method no. 1; 4 days; Fig. 1H) and the S1-modETV2 method. For this comparison, we used three independent h-iPSC clones corresponding to three different cellular origins: dermal FBs [clone FB(1)-iPSC-C3], umbilical cbECFCs [cbECFC(4)-iPSC-C9], and uEPs [uEP(5)-iPSC-C11] (Fig. 1H). Examination of the efficiency revealed that all four S1-S2 differentiation protocols produced significantly lower efficiencies than the S1-modETV2 method. Moreover, depending on the h-iPSC clone used, there was a wide variation in efficiency among the four S1-S2 methods, with h-iECs ranging from ~3 to ~70% (Fig. 1H). In contrast, differentiation under the S1-modETV2 protocol produced significantly higher efficiencies (89 to 95%) and eliminated inconsistencies between clones.

Inefficient activation of endogenous *ETV2* in intermediate h-MPCs

To further evaluate the issue of inefficiency, we carried out a transcriptional examination of the standard S1-S2 differentiation protocol. As expected, conversion of h-iPSCs into h-MPCs coincided with transient activation of mesodermal transcription factors *MIXL1* and *TBXT* (Fig. 2A and fig. S3A). Likewise, differentiation of h-MPCs into h-iECs involved activation of *ETV2* (transiently) and then *ERG* (Fig. 2A and fig. S3A), consistent with previous vascular developmental descriptions (*6*, *20*). However, there were significant differences when comparing the efficiencies of transcription factor activation. On one hand, activation of *TBXT* (which encodes for Brachyury) was robust and highly uniform at 48 hours (~97% $Brachyury^+$ cells; Fig. 2B), suggesting that the conversion of h-iPSCs into h-MPCs is unlikely to account for the large inefficiency observed in the S1-S2 protocol. On the other hand, *ETV2* activation by 72 hours was limited and far from uniform (~33% $ETV2^+$ cells; Fig. 2C), indicating inefficient conversion of h-MPCs into h-iECs. Control h-iPSCs in which *ETV2* was genetically abrogated using CRISPR-Cas9 (h-iPSC-$ETV2^{-/-}$) displayed unaltered *TBXT* activation and mesodermal conversion but were unable to activate *ETV2* and, in turn, incapable of initiating S2 (Fig. 2, B and C, and fig. S4, D and E). Because *ETV2* expression is governed by VEGF signaling (*21*), we examined whether increasing the concentration of supplemented VEGF could improve its inefficient activation during S1-S2. However, we found that beyond 50 ng/ml, VEGF failed to further increase the proportion of $ETV2^+$ cells and thus the subsequent conversion to $CD31^+$ h-iECs (Fig. 2D and fig. S4, G and H).

Collectively, we found that while conversion of h-iPSCs into $TBXT^+$ h-MPCs occurs very efficiently (>95%), activation of endogenous *ETV2* in h-MPCs is clearly limited (~30%) during the S1-S2 protocol and did not improve by simply increasing VEGF concentration. Thus, we concluded that to improve the conversion of h-iPSCs into h-iECs, emphasis should be put on finding alternative means to effectively activate *ETV2* in the intermediate h-MPCs.

Transient expression of exogenous *ETV2* uniformly converts h-MPCs into h-iECs

Our approach to more uniformly activate *ETV2* in h-MPCs is to use modRNA. Six hours after transfection of h-MPCs with modRNA(ETV2), >85% of the cells expressed ETV2 (Fig. 2E), a significant increase from the mere ~30% observed in the S1-S2 protocol. Notably, h-iPSC-$ETV2^{-/-}$ also displayed widespread ETV2 expression after transfection, indicating that activation was independent of endogenous *ETV2* (Fig. 2E). This robust expression of *ETV2* produced high rates of endothelial specification and efficient conversion into h-iECs in both unmodified h-iPSCs and h-iPSC-$ETV2^{-/-}$ with the S1-modETV2 differentiation protocol (Fig. 2F). In contrast, with the S1-S2 protocol, the differentiation process was less efficient and completely dependent on endogenous *ETV2* expression (h-iPSC-$ETV2^{-/-}$ failed to produce h-iECs) (Fig. 2F and fig. S4F). Moreover, the S1-modETV2

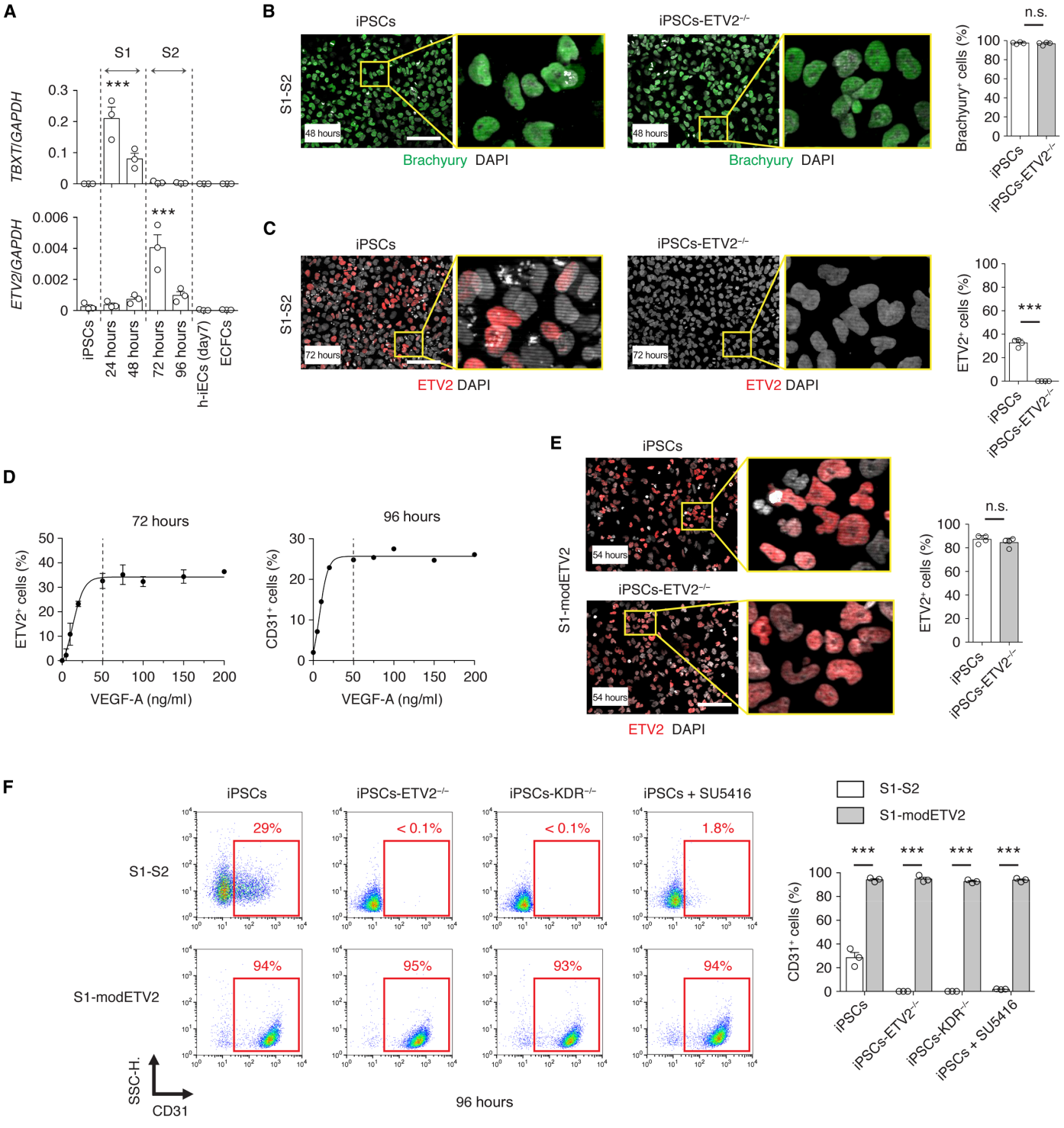

Fig. 2. Inefficient activation of endogenous *ETV2* in intermediate h-MPCs during the standard S1-S2 differentiation protocol. (**A**) mRNA expression of *TBXT* and *ETV2* during the S1-S2 differentiation protocol. Data normalized to *GAPDH* expression. (**B**) Brachyury expression during the S1-S2 protocol. h-iPSCs lacking endogenous *ETV2* (h-iPSCs-ETV2$^{-/-}$) served as control. Percentage of Brachyury^{+} cells at 48 hours. (**C**) ETV2 expression during the S1-S2 protocol. Percentage of ETV2^{+} cells at 72 hours. (**D**) Effect of VEGF-A concentration on the percentages of ETV2^{+} cells at 72 hours (immunofluorescence staining) and CD31^{+} cells at 96 hours (flow cytometry) during the S1-S2 protocol. (**E**) Immunofluorescence staining for ETV2 in h-iPSCs during the S1-modETV2 protocol. h-iPSCs-ETV2$^{-/-}$ served as control. Percentage of ETV2^{+} cells after transfection with modRNA. (**F**) Conversion efficiency of h-iPSCs into CD31^{+} h-iECs by flow cytometry. Comparison of the S1-S2 and the S1-modETV2 protocols. h-iPSCs-ETV2$^{-/-}$, h-iPSCs-KDR$^{-/-}$, and h-iPSCs treated with the VEGF receptor 2 inhibitor SU5416 served as controls. SSC-H, side scatter height. In (B), (C), and (E), nuclei stained by DAPI. Scale bar, 100 μm. Bars represent means ± SD; $n = 4$; n.s., no statistical differences; and ***$P < 0.001$ between h-iPSCs and h-iPSCs-ETV2$^{-/-}$. In (F), $n = 3$; ***$P < 0.001$ between indicated groups.

protocol maintains the differentiation process in the absence of VEGF receptor 2 (VEGFR2) expression. h-iPSCs in which *KDR* (which encodes for VEGFR2) was genetically abrogated using CRISPR-Cas9 (h-iPSC-KDR$^{-/-}$) displayed an unaltered ability to differentiate into h-iECs (93% at 96 hours) with the S1-modETV2 method but were incapable of differentiating (<0.1%) with the standard S1-S2 protocol (Fig. 2F and fig. S4, A to C). Likewise, chemical abrogation of VEGFR2 signaling with the inhibitor SU5416 impaired the differentiation of h-iPSCs into h-iECs with the S1-S2 protocol but not with the S1-modETV2 protocol (<2 and 94% h-iECs at 96 hours, respectively) (Fig. 2F).

Together, we showed that delivery of modRNA(ETV2) is an effective means to robustly and transiently express ETV2 in intermediate h-MPCs, which, in turn, initiates widespread conversion into h-iECs. Our S1-modETV2 protocol renders the differentiation process independent of VEGFR2 expression and of endogenous ETV2, thus overcoming one of the main limitations in current protocols.

Time of ETV2 activation affects the transcriptional profile of h-iECs

Previous studies have suggested that directly inducing *ETV2* expression on h-iPSCs could generate h-iECs without transition through an intermediate mesodermal stage (*14*). However, it remains unclear whether this strategy produces functionally competent h-iECs. To address this question, we generated putative h-iECs by transfecting h-iPSCs with modRNA(ETV2) (protocol here referred to as early modETV2) (Fig. 3A). This method rapidly and efficiently converted h-iPSCs into CD31$^+$ cells (Fig. 3B and fig. S5), which is consistent with previous reports (*16*). Moreover, conversion was dependent on the concentration of modRNA(ETV2) and reproducible in all h-iPSCs clones tested, irrespective of the donor and cellular origin of the clones (fig. S5, C and D). Transfection of h-iPSCs with modRNA(ETV2) enabled early and transient expression of ETV2 (fig. S5, E and F), which occurred without previous significant expression of TBXT, suggesting a bypass of the intermediate mesodermal stage (fig. S6). With this approach, there was a remnant of undifferentiated (non-transfected) CD31$^-$/OCT4$^+$ cells at 48 hours, which was deemed undesirable (fig. S5E). Nonetheless, repeated subculture and purification of CD31$^+$ cells largely mitigated this concern.

To further elucidate potential differences between h-iECs generated from our S1-modETV2, the S1-S2, and the early modETV2 protocols, we performed RNA sequencing (RNA-seq) analysis across multiple h-iEC samples generated from three independent h-iPSC lines using all three differentiation protocols. Human ECFCs and the parental undifferentiated h-iPSCs served as positive and negative controls, respectively. Globally, there were thousands of differentially expressed genes across all the h-iEC groups (Fig. 3C and fig. S7A). Nevertheless, hierarchical clustering analysis of differentially expressed genes revealed (i) proximity between all the h-iEC groups and (ii) that h-iECs were transcriptionally closer to ECFCs than to h-iPSCs (Fig. 3F). These patterns of hierarchical association were confirmed by pairwise correlation (Fig. 3D) and principal components analyses (Fig. 3E). Moreover, analysis of selected endothelial and pluripotent genes confirmed that all groups of h-iECs were transcriptionally more consistent with an endothelial phenotype than with the parental pluripotent state (Fig. 3G and fig. S7B) (please note that Fig. 3G is not intended as a comprehensive list of EC genes). Our analysis also revealed that among h-iECs, there was more transcriptional proximity between h-iECs generated from the standard S1-S2 protocol and our S1-modETV2 method (Pearson's correlation coefficient $r = 0.987$) than between h-iECs derived from the early modETV2 protocol and the other h-iEC groups (Fig. 3D).

To gain more insight into the transcriptional differences, we carried out gene ontology (GO) enrichment analysis between h-iECs generated with our S1-modETV2 and the early modETV2 differentiation protocols. Notably, analysis of all differentially expressed genes revealed that h-iECs generated with our S1-modETV2 displayed significant enrichment in genes associated with positive regulation of cell migration (fig. S7C). Moreover, a GO analysis was performed with differentially expressed genes from EC clusters 5 and 10 (cluster elucidated by hierarchical clustering analysis; Fig. 3F). Results indicated positive enrichment in h-iECs generated with our S1-modETV2 of genes associated with not only cell migration but also angiogenesis and smooth muscle proliferation (Fig. 3H and fig. S7D), suggesting differences in genes affecting critical vascular function.

Early activation of ETV2 renders putative h-iECs with impaired functionality

Next, we examined whether the transcriptional differences observed between h-iECs generated from different protocols affected their capacity to function as proper ECs. Specifically, we compared h-iECs that were generated with the standard S1-S2, our S1-modETV2, and the early modETV2 protocols. Notably, ETV2 expression is transient in both differentiation protocols, and thus at the time of h-iEC characterization, ETV2 expression was completely absent (Fig. 1, D and E). Human cbECFCs served as control for bona fide ECs. First, we assessed the capacity to grow in culture. Previous studies have shown mixed results with regard to the expansion potential of h-iECs, and currently, there is no consensus on this issue (*22*). We observed that h-iECs generated with our S1-modETV2 protocol were easily expanded in culture for a period of 3 weeks, with an average expansion yield of ~70-fold (Fig. 4A). This yield was significantly higher than that of h-iECs produced with the S1-S2 differentiation protocol (~20-fold), which was mainly attributed to differences in efficiency during the initial 4 days of differentiation (Fig. 4A). More notable, however, was the lack of expansion displayed by h-iECs generated with the early modETV2 protocol. Notwithstanding the high differentiation efficiency of this method (Fig. 3A), these putative h-iECs ceased proliferating after approximately 2 weeks in culture with only a modest overall yield of ~2-fold (Fig. 4A). We also measured Ki67 expression (a nuclear protein associated with cellular proliferation) on day 7 in h-iECs generated by the three differentiation protocols and found statistically significant differences between S1-S2 (46.8% Ki67$^+$ cells), S1-modETV2 (53.5%), and early ETV2 (14.8%) (Fig. 4A). In addition, it is important to note that h-iECs obtained by the S1-modETV2 method retained an endothelial phenotype, with typical cobblestone-like morphology along their expansion in culture, did not express the pluripotent marker *OCT4*, expressed numerous EC markers at the mRNA and protein levels, and showed affinity for the binding of *Ulex europaeus agglutinin I* (UEA-I) lectin (fig. S8). Although it is certainly possible that further maturation occurs during expansion in vitro, h-iECs fundamentally remained endothelial when one considers a plethora of EC markers, even though the level of expression of some individual genes (such as *NOS3* and *vWF*) varied over time (fig. S8C). Examination at days 4, 11, and 21 during expansion revealed that h-iECs remained fairly pure (>95% VE-Cadherin$^+$/CD31$^+$ cells), maintained expression of EC markers at the mRNA and protein levels, and remained negative for *POU5F1* (OCT4) and α–smooth muscle actin (α-SMA) (fig. S8D).

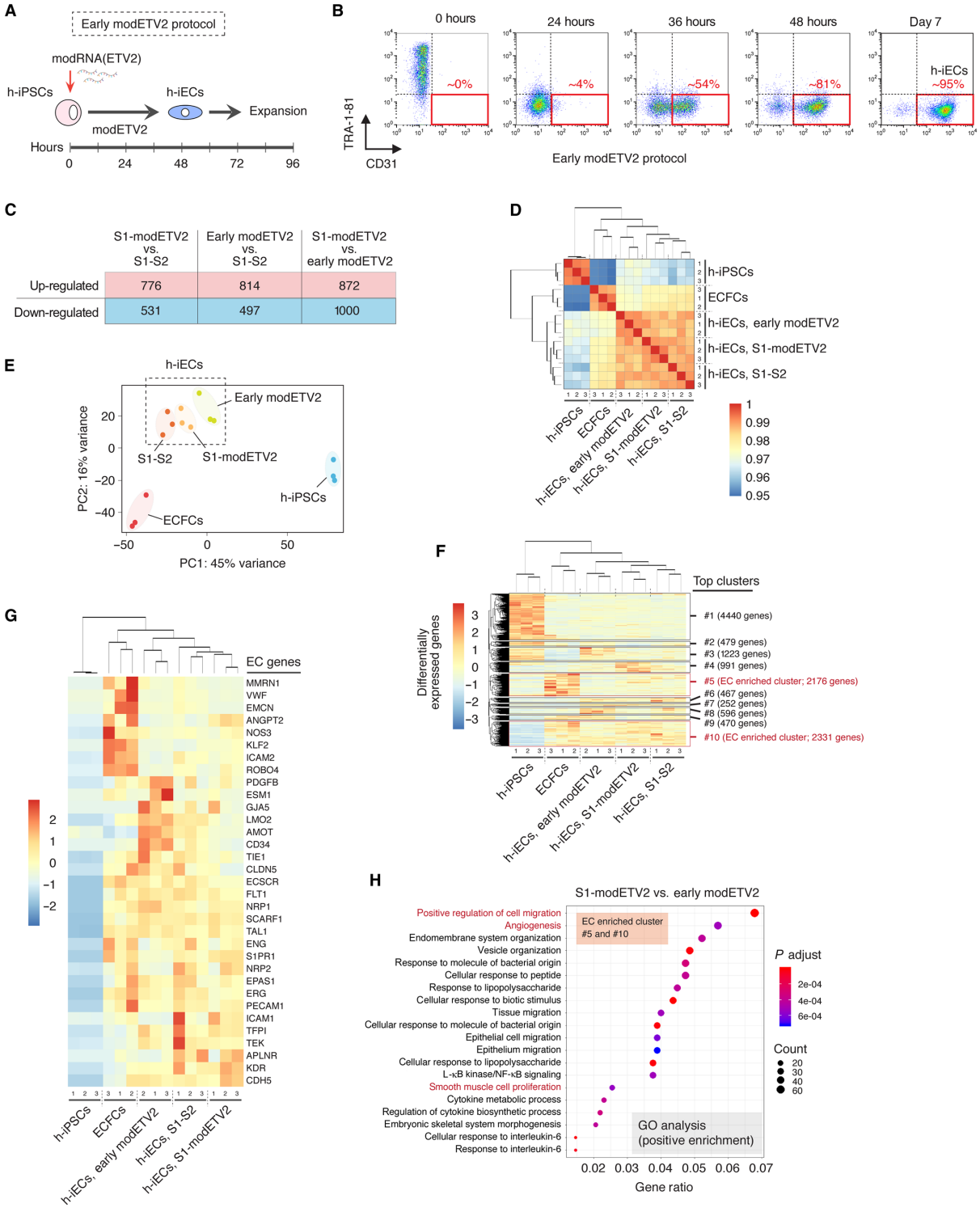

Fig. 3. Transcriptional analysis of h-iECs obtained from various differentiation protocols. (**A**) Schematic of protocol for early transfection of h-iPSCs with modRNA encoding *ETV2*. (**B**) Conversion efficiency h-iPSCs into CD31$^+$ cells by flow cytometry using the early modETV2 protocol. (**C** to **H**) RNA-seq analysis across multiple h-iEC samples generated from three independent h-iPSC lines using all three differentiation protocols. Human ECFCs and the parental undifferentiated h-iPSCs served as positive and negative controls, respectively. (C) Number of differentially expressed genes between h-iEC samples from each differentiation protocol. (D) Pairwise correlation based on Pearson coefficients between all samples. (E) Principal components (PC) analysis. (F) Heat map and hierarchical clustering analysis of global differentially expressed genes. (G) Heat map and hierarchical clustering analysis of selected EC-specific genes. (H) Gene ontology analysis between h-iECs generated with the S1-modETV2 and the early modETV2 differentiation protocols. Analysis carried out with differentially expressed genes from EC clusters 5 and 10 based on (F). Genes displayed correspond to positive enrichment for h-iECs generated with the S1-modETV2 protocol.

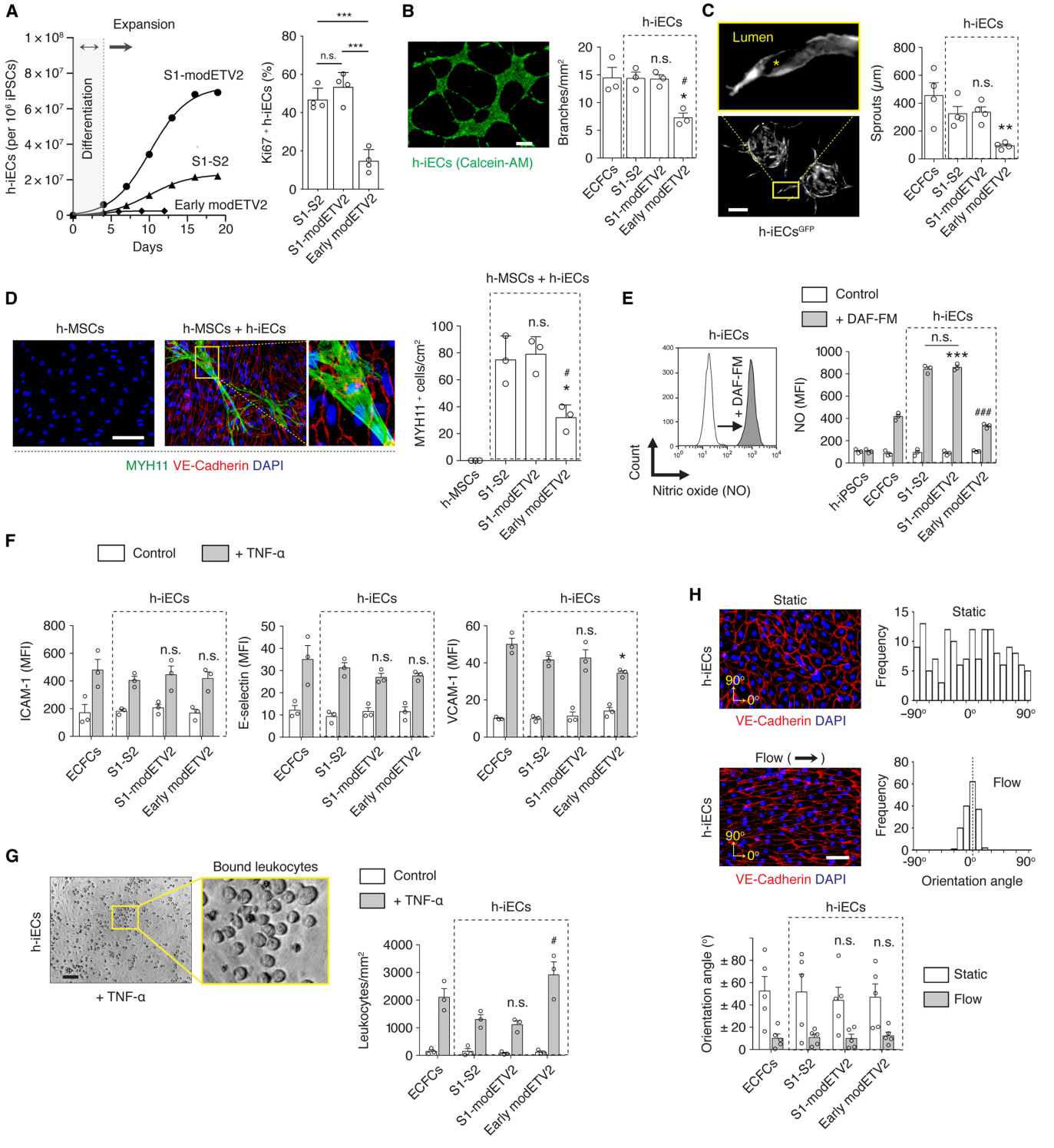

Fig. 4. Functional properties of h-iECs. Comparison of h-iECs generated by the S1-S2, S1-modETV2, and early modETV2 protocols. (**A**) Expansion curves for h-iECs, starting with 10^6 h-iPSCs. Percentage of Ki67$^+$ h-iECs on day 7 is shown. (**B**) Capillary-like network formation assay. Live cells stained by Calcein-AM are shown. (**C**) Sprouts formation assay using h-iECs^{GFP} spheroids embedded in fibrin gel. (**D**) Induction of smooth muscle cell differentiation of h-MSCs by h-iECs. Differentiation was assessed by smooth muscle myosin heavy chain 11 (MYH11). (**E**) NO production measured by flow cytometry upon exposure to 4-amino-5-methylamino-2′,7′-difluorofluorescein diacetate (DAF-FM). MFI, mean fluorescence intensity. (**F**) Leukocyte adhesion molecules ICAM-1, E-selectin, and VCAM-1 measured by flow cytometry upon exposure to TNF-α. Cells not exposed to TNF-α served as control. (**G**) Bound leukocytes upon exposure to TNF-α. (**H**) Alignment of h-iEC under static and flow conditions. 0° represents the direction of flow. In all panels, bars represent means ± SD; $n = 3$; $^*P < 0.05$, $^{**}P < 0.01$, $^{***}P < 0.001$ between h-iECs and ECFCs. #$P < 0.05$, ###$P < 0.001$ compared to S1-S2 protocol. n.s., no statistical differences compared to both ECFCs and S1-S2 protocol. Scale bars, 200 μm [(B) and (C)], 100 μm [(D) and (H)], and 50 μm [(G)].

We then evaluated the performance of h-iECs using an array of standard endothelial functional assays, including ability to (i) assemble into capillary-like structures (Fig. 4B), (ii) launch angiogenic sprouts with proper lumens (Fig. 4C), (iii) induce smooth muscle differentiation of human mesenchymal stem cells (h-MSCs) (Fig. 4D), (iv) produce nitric oxide (NO) (Fig. 4E), (v) up-regulate expression of leukocyte adhesion molecules [E-selectin, intercellular adhesion molecule–1 (ICAM-1), and vascular cell adhesion molecule–1 (VCAM-1)] upon exposure to tumor necrosis factor–α (TNF-α) (Fig. 4F), (vi) up-regulate leukocyte binding upon exposure to TNF-α (Fig. 4G), and (vii) sense and adapt to shear flow, aligning to the direction of flow (Fig. 4H). Collectively, this comprehensive examination confirmed that h-iECs generated with both the S1-S2 and our S1-modETV2 differentiation protocols were functionally very similar, with no statistically significant differences between both groups in any of the assays (Fig. 4, B to H). In addition, both h-iEC groups were comparable to the control ECFCs (the only exception was higher NO production by h-iECs; $P < 0.001$; Fig. 4E), thus suggesting adequate endothelial function. In contrast, h-iECs generated with the early modETV2 protocol showed signs of impaired functionality. When compared to the control ECFCs, these h-iECs appeared competent in some fundamental capacities such as the ability to regulate leukocyte adhesion upon an inflammatory stimulus and the capacity to align in the direction of flow. However, h-iECs generated with the early modETV2 protocol displayed quantitative deficiencies in several important respects, including a significantly lower ability to assemble into capillary-like structures ($P < 0.05$; Fig. 4B), to launch proper angiogenic sprouts ($P < 0.01$; Fig. 4C), and to induce smooth muscle differentiation of h-MSCs ($P < 0.05$; Fig. 4D). These differences were also statistically significant when compared to h-iECs generated with both the S1-S2 and our S1-modETV2 differentiation protocols, suggesting certain fundamental phenotypic differences between h-iECs generated from the different protocols.

Timely activation of ETV2 is critical for proper vascular network–forming ability

Last, we examined the capacity of the different h-iECs to assemble into functional blood vessels in vivo (Fig. 5). To this end, we used our model of vascular network formation in which human ECs are combined with supporting MSCs in a hydrogel, and the grafts are then implanted into immunodeficient nonobese diabetic (NOD)–severe combined immunodeficient (SCID) mice (*23*). After 7 days in vivo, macroscopic examination of the explants suggested differences in the degree of vascularization between implants containing different types of h-iECs ($n = 5$) (Fig. 5A). Histological [hematoxylin and eosin (H&E)] analysis revealed that grafts with h-iECs generated with the S1-modETV2 protocol had an extensive network of perfused microvessels (Fig. 5B, left). These microvessels were primarily lined by the h-iECs, as confirmed by the expression of human-specific CD31 (Fig. 5E, left) and mouse-specific CD31 (Fig. 5G), by the affinity for UEA-I (Fig. 5D, left), and by the use of GFP (green fluorescent protein)–labeled h-iECs (fig. S9D). Moreover, these human lumens contained mouse erythrocytes (Fig. 5B, left), indicating formation of functional anastomoses with the host circulatory system. The presence of perfusion was further assessed by the infusion of biotinylated UEA-I, which specifically bounded to the lumen of the human blood vessels, confirming that they were connected to the mouse circulation (Fig. 5H). In contrast, the number of perfused human vessels in grafts with h-iECs generated with the early modETV2 protocol was exceedingly low (Fig. 5B, right). These h-iECs remained organized as lumenal structures (Fig. 5, D and E, right), but the lumens were rarely perfused (Fig. 5B, right). Microvessel density in grafts containing h-iECs from the early modETV2 protocol was significantly lower than in any other group (Fig. 5C). Notably, there were no significant differences in vessel density between grafts formed with h-iECs from the S1-modETV2 protocol, the S1-S2 protocol (both of which underwent transition through mesodermal intermediates), and the control ECFCs.

It is important to note that although cotransplantation with MSCs facilitates engraftment, h-iECs derived from the S1-modETV2 protocol were also able to engraft and form perfused vessels when implanted alone, without MSCs (fig. S9). Grafts containing h-iECs alone became vascularized in 7 days, and histological analysis confirmed the presence of numerous microvessels lined by the h-iECs (fig. S9, A to C).

We also examined the presence of mural cell investment around the newly formed human vessels, a hallmark of proper vessel maturation and stabilization (*24*). There was a notable difference between h-iECs generated with the S1-modETV2 protocol and those generated with the early modETV2 with regard to perivascular investment (Fig. 5, D to F). In grafts with h-iECs from the S1-modETV2 protocol, the large majority (~87%) of the human vessels had proper coverage by perivascular cells expressing α-SMA (Fig. 5, D and E, left, and F). This high percentage of perivascular coverage is to be expected by day 7 in this model (*25*), and vessels formed by control ECFCs consistently displayed high coverage (Fig. 5F). In contrast, grafts containing h-iECs from the early modETV2 protocol had only ~8% of their human vessels covered by $\alpha\text{-SMA}^+$ cells (Fig. 5, D and E, right, and F). These h-iECs were able to engraft and self-assemble into recognizable lumenal structures, but these structures lacked perivascular cells indicating inadequate maturation. Moreover, TUNEL (terminal deoxynucleotidyl transferase–mediated deoxyuridine triphosphate nick end labeling) staining of explants at day 7 revealed signs of apoptosis in a large percentage of human vessels lined by h-iECs from the early modETV2 protocol (Fig. 5J), an indication of vessel instability. On the other hand, 30 days after implantation, grafts that used h-iECs generated with the S1-modETV2 protocol still contained extensive and uniform networks of human vessels with proper perivascular coverage (Fig. 5I).

All together, we demonstrated that during the differentiation of h-iPSCs into h-iECs, the ETV2 activation stage is critical. With our optimized S1-modETV2 protocol, activation of ETV2 occurred at the intermediate mesodermal stage, which produced h-iECs that were phenotypically and functionally competent. However, bypassing transition through the mesodermal stage by early activation of ETV2 produced putative h-iECs with a transcriptional profile further away from that of bona fide ECs and, more importantly, with impaired functionality.

DISCUSSION

Here, we developed a novel protocol that enables highly efficient differentiation of h-iPSCs into competent h-iECs. The protocol entails a total differentiation period of 4 days and comprises two steps: (i) differentiation of h-iPSCs into intermediate h-MPCs and (ii) conversion of h-MPCs into h-iECs upon delivery of modRNA encoding *ETV2*. We showed that this S1-modETV2 approach allows widespread expression of ETV2 throughout the entire h-MPC population, thus overcoming one of the main hurdles of current protocols. Using our

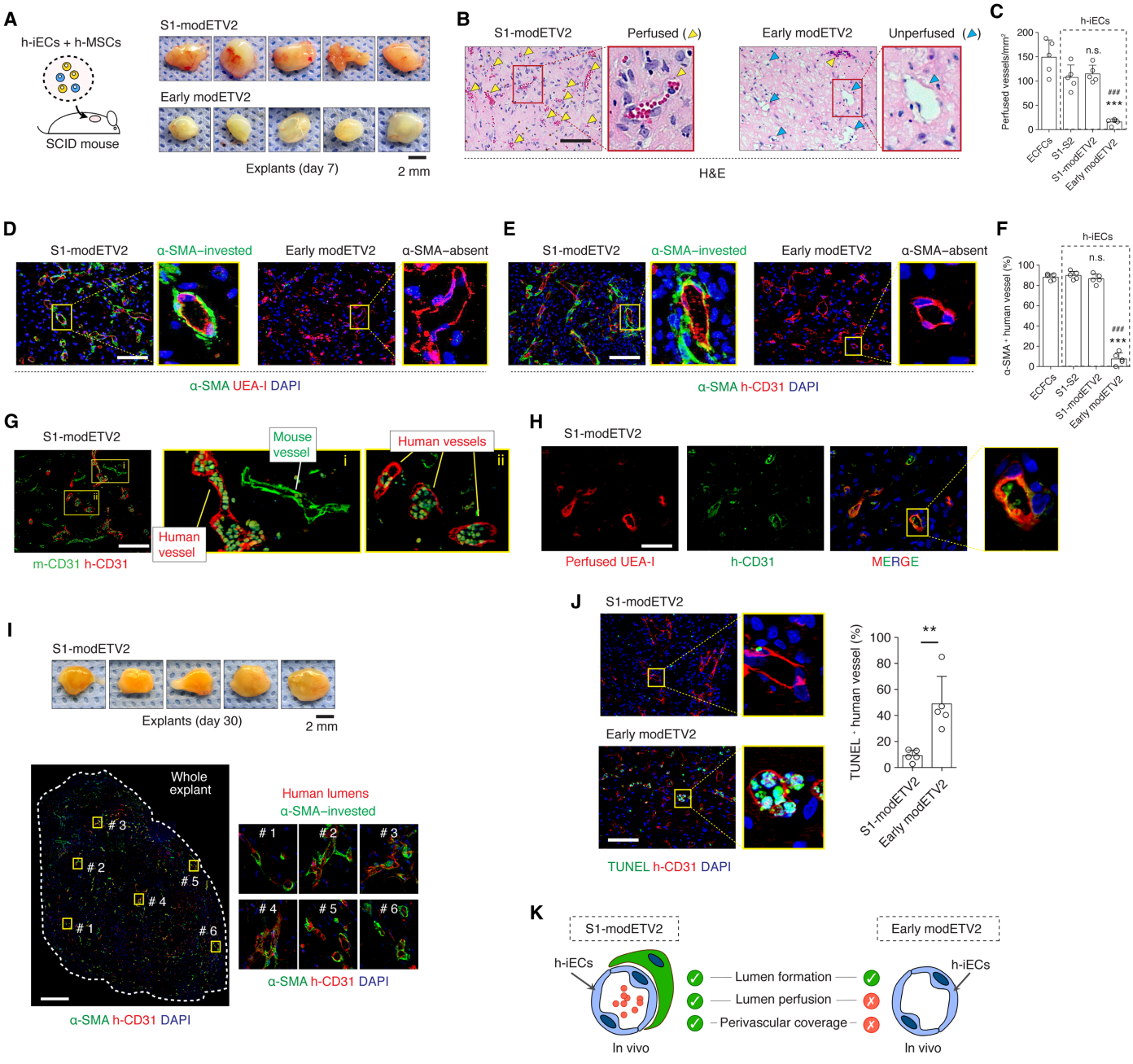

Fig. 5. In vivo vascular network–forming ability of h-iECs. Comparison of grafts containing h-iECs generated by different protocols. (**A**) Macroscopic views of grafts explanted at day 7. (**B**) H&E staining of grafts at day 7. (**C**) Microvascular density on day 7. (**D** and **E**) Immunofluorescence staining at day 7. Human lumens stained by (D) UEA-I and (E) h-CD31 antibody. Perivascular coverage stained by α-SMA antibody. (**F**) Human lumens with α-SMA$^+$ perivascular coverage at day 7. (**G**) Human and mouse vessels distinguished by m-CD31 and h-CD31 antibodies. (erythrocytes within the lumens had green autofluorescence). (**H**) Perfused human vessels detected by infused UEA-I and h-CD31 antibody. (**I**) Macroscopic views and immunofluorescence staining of grafts with h-iECs (S1-modETV2 protocol) at day 30. (**J**) TUNEL and h-CD31 staining of grafts at day 7. (**K**) Schematic of in vivo vascular network–forming ability of h-iECs. Bars represent means ± SD; $n = 5$. In (C) and (F), $^{***}P < 0.001$ compared to ECFCs; $^{###}P < 0.001$ compared to S1-S2. n.s., no statistical differences compared to both ECFCs and S1-S2. In (J), $^{**}P < 0.01$. Scale bars, 100 μm [(B), (D), (E), (G), and (J)], 50 μm (H), and 500 μm (I). Photo credit: Kai Wang, Boston Children's Hospital.

customized protocol, we reproducibly and efficiently differentiated 13 different h-iPSC clonal lines into h-iECs. In all cases, we produced h-iECs at exceedingly high purity irrespective of the h-iPSC donor and cellular origin, and there were no statistical differences in efficiency. Notably, this high efficiency and reproducibility were absent when we used the standard S1-S2 protocol, which relies on VEGF signaling for endogenous *ETV2* activation. In addition, we were able to expand the resulting h-iECs with ease, obtaining an average h-iEC–to–h-iPSC ratio of ~70-fold after 3 weeks in culture. We demonstrated that our h-iECs were phenotypically, transcriptionally, and functionally consistent

with bona fide ECs, including a robust ability to form perfused vascular networks in vivo.

Over the past decade, refinements to the standard S1-S2 differentiation protocol have steadily improved efficiency. Improvements have included, for example, the inhibition of the Notch and the transforming growth factor–β signaling pathways, the activation of protein kinase A, or the synergistic effects of VEGF and bone morphogenetic protein 4 (BMP4) during S2 (*18*, *19*, *26*). However, most of these advances have been largely incremental, and consensus holds that the differentiation of h-iPSCs into h-iECs remains somewhat inconsistent (*27*). The incorporation of BMP4 during S2 was shown to produce a significant improvement in differentiation efficiency; however, the mechanism behind this improvement remains unknown, and thus, it is unclear whether this approach can consistently produce high efficiency across multiple clonal iPSC lines, independently of their cellular origin (*18*). One of the major difficulties is related to the necessary transition through the intermediate h-MPCs, which serve as common progenitors not only to h-iECs but also to other end-stage mesodermal cell types (*28*, *29*). Thus, directing h-MPCs to solely differentiate into h-iECs is a challenge. A recent study that used single-cell RNA analysis revealed that after S1-S2, non-EC populations (including cardiomyocytes and vascular smooth muscle cells) were in fact predominant among the differentiated cells, and less than 10% were actually identified as bona fide ECs (*3*). Studies have also shown that EC specification is dictated by a transient activation of *ETV2*, which, in turn, depends on VEGF signaling (*21*, *30*). However, our study has revealed that the activation of endogenous *ETV2* during S2 is inherently inefficient and that increasing the concentration of VEGF can only improve this constraint to a certain degree. This limited ability of exogenous VEGF to enhance efficiency could be explained by the fact that VEGF has also been shown to promote h-iPSC differentiation into other mesodermal fates, including cardiac progenitor cells, cardiomyocytes, and hepatic-like cells (*3*, *28*, *31*–*33*). Thus, to improve efficiency, VEGF activation of *ETV2* must be accompanied by inhibition of all other competing fates, which is not trivial. Our approach, however, circumvents this challenge. By using modRNA, we were able to transiently express ETV2 in a high percentage of h-MPCs and independently of the presence of exogenous VEGF. This, in turn, allowed widespread conversion into h-iECs, thereby eliminating the problem of inefficiency. In addition, our study provides an important new insight: that timely activation of *ETV2* is critical and that bypassing the intermediate mesodermal stage is detrimental. h-iECs generated by our S1-modETV2 methodology displayed proper blood vessel–forming ability in vivo, whereas putative h-iECs generated by the early modETV2 approach displayed impaired functionality and were unable to robustly form perfused vessels with adequate perivascular stability (Fig. 5K).

Current protocols are also limited by inconsistent results among different h-iPSC lines. A recent study examined genetically identical h-iPSC clonal lines that were derived from various tissues of the same donor and found that by following the standard S1-S2 protocol, both differentiation efficiency and gene expression of the resulting h-iECs varied significantly depending on the source of h-iPSCs (*5*). In our study, we have also found inconsistencies in differentiation efficiency between h-iPSC clonal lines with different cellular origins, including lines with identical genetic makeup and lines derived from the same tissues in different donors. This lack of consistency is certainly undesirable from a clinical translation standpoint (*22*). Also, dependency on cellular origin may explain why published results on differentiation efficiency are often mixed and rely on selecting h-iPSC clones that are particularly attuned to EC differentiation. Our method eliminates this uncertainty as it consistently produces high efficiency, irrespective of the donor and cellular origin from which the h-iPSC clones are derived.

In summary, we have developed a protocol that enables highly efficient and reliable differentiation of h-iPSCs into competent h-iECs. The protocol is simple, rapid, and entails delivery of modRNA encoding the transcription factor *ETV2* at the intermediate mesodermal stage of differentiation. In terms of added benefits, our method provides two key advantages over current published protocols. First, it significantly increases reproducibility among different clones of h-iPSCs and thus eliminates the need for selecting clones that are particularly attuned to activation of endogenous *ETV2* during differentiation. Second, our method yields exceedingly high differentiation efficiency (>90%) in just 4 days, reducing the need for additional purification or enrichment steps. Hence, our method could be not only cost effective but also resource saving when manufacturing ECs for regenerative medicine. In addition, it is important to note that modRNA vectors are nonviral, nonintegrating, and inherently transient, which, from a translational standpoint, is also beneficial. We anticipate that our protocol could have broad application in regenerative medicine because it provides a reliable means to obtain autologous h-iECs for vascular therapies. The advent of high-throughput electroporation systems, as well as advances in scalability and clinical-grade materials, should enable further refinements to this protocol for the generation of clinical-grade h-iECs.

MATERIALS AND METHODS

Isolation and culture of h-MSCs, human ECFCs, and uEPs

h-MSCs were isolated from the white adipose tissue as previously described (*34*). h-MSCs were cultured on uncoated plates using MSC medium: MSCGM (Lonza, catalog no. PT-3001) supplemented with 10% GenClone fetal bovine serum (FBS; Genesee, catalog no. 25-514) and 1× penicillin-streptomycin-glutamine (PSG, Thermo Fisher Scientific, catalog no. 10378106). All experiments were carried out with h-MSCs between passages 6 and 10. Human ECFCs were isolated from umbilical cord blood samples in accordance with an Institutional Review Board–approved protocol as previously described (*35*). All ECFCs were derived from umbilical cord blood samples obtained from normal term deliveries. Samples were collected ex utero using heparinized tubes. ECFCs were cultured on 1% gelatin-coated plates using ECFC medium: Endothelial Cell Growth medium 2 (except for hydrocortisone; PromoCell, catalog no. C22111) supplemented with 10% FBS and 1× PSG. All experiments were carried out with ECFCs between passages 6 and 8. Human uEPs were isolated from urine samples and were cultured on 1% gelatin-coated plates using ECFC medium. All experiments were carried out with uEPs up to passage 4.

Generation and culture of h-iPSCs

h-iPSCs were generated via nonintegrating episomal transferring of selected reprogramming factors (Oct4, Sox2, Klf4, L-Myc, and Lin28). Briefly, four plasmids encoding h-oct4, h-sox2, h-klf4, h-myc, h-lin-28, and EBNA-1 (Addgene plasmid nos. 27077, 27078, 27080, and 37624 deposited by S. Yamanaka) were introduced via electroporation into h-MSCs, ECFCs, and uEPs. Transfected cells were then cultured with mTeSR-E7 medium (STEMCELL Technologies, catalog no. 05910).

h-iPSC colonies spontaneously emerged between days 15 and 25. Colonies were then picked and transferred to a Matrigel-coated (Corning, catalog no. 354277), feeder-free culture plate for expansion and were routinely checked for absence of mycoplasma. h-iPSCs were cultured in mTeSR1 medium (STEMCELL Technologies, catalog no. 85850) on six-well plates coated with Matrigel. At 80% confluency, h-iPSCs were detached using TrypLE Select (Thermo Fisher Scientific, catalog no. 12563-029) and split at a 1:6 ratio. Culture media were changed daily. h-iPSC phenotype was validated by expression of pluripotent transcription factors OCT4, NANOG, and SOX2 and by the ability to form teratomas. Teratoma formation assay was performed by injecting 1 million h-iPSCs mixed in 100-μl Matrigel into the dorsal flank of nude mice (Jackson laboratory). Four weeks after the injection, tumors were surgically dissected from the mice, weighed, fixed in 4% formaldehyde, and embedded in paraffin for histology. Sections were stained with H&E.

Electroporation

Electroporation was routinely used to introduce plasmids, modRNA, and proteins into the cells as described for each experiment. Electroporation was carried out with a Neon electroporation system (Thermo Fisher Scientific). Unless specified otherwise, electroporation parameters were set as 1150 V for pulse voltage, 30 ms for pulse width, 2 for pulse number, 3 ml of electrolytic buffer, and 100-μl resuspension buffer R in 100-μl reaction tips (Thermo Fisher Scientific, catalog no. MPK10096).

Establishment of *KDR* and *ETV2* knockout h-iPSC lines

Alt-R CRISPR-Cas9 system [Integrated DNA Technologies (IDT)] was used to knock out *KDR* [guide RNA (gRNA): ACGGACTGTACCATTTCGTG; off-target score: 76] and *ETV2* (gRNA: GAGCCTACAAGTGCTTCTAC; off-target score: 92) in h-iPSCs. Briefly, gRNA was prepared by mixing cripsr RNA (crRNA) and trans-activating crispr RNA (tracrRNA) (IDT, catalog no. 1072533) to a final duplex concentration of 40 μM. Ribonucleoprotein (RNP) complex was prepared with 1-μl volume of 61 μM Cas9 protein (IDT, catalog no. 1074181) complexed with 2.5 μl of gRNA for 15 min at room temperature (RT). Following incubation, RNP complexes were diluted with 100-μl R buffer and mixed with 1 million pelleted h-iPSCs for electroporation. Two days later, h-iPSCs were dissociated into single cells and plated at 2000 cells per 10-cm dish in mTeSR1 supplemented with CloneR (STEMCELL Technologies, catalog no. 5888). Single cells were able to grow and form single visible colonies after 10 days. Forty-eight colonies were randomly picked on the basis of morphology and were then mechanically disaggregated and replated into individual wells of 48-well plates. Colonies were then expanded in culture as described above. To validate the knockout (KO) genes in each clone, genomic DNA templates were prepared by lysing cells in QuickExtract DNA extraction solution (Lucigen, catalog no. QE0905T). Target regions were amplified by using specific polymerase chain reaction (PCR) primers (ETV2_F: CACTCGGGATCCGTTACTCC; ETV2_R: GTTCGGAGCAAACGGTGAGA; KDR_F: CAAGCCCTTTGTTGTACTCAATTCT; KDR_R: ATTAATTTTTCAGGGGACAGAGGGA) and the KAPA HiFi HotStart PCR kit (KAPA Biosystems, catalog no. KK2601). Sanger sequencing (Genewiz) was performed to identify mutant clones. To analyze potential off-target effects of KDR gRNA-targeted KO, the top 10 off-target sites were predicted by an algorithm provided by IDT. Next, 500–base pair (bp) amplicons covering the position of these potential off-target sites were amplified by PCR, and then Sanger sequencing was applied (Genewiz) to identify any nucleotide base mutations within the amplicons (fig. S4C).

Establishment of h-iPSC line expressing GFP

h-iPSCs were dissociated and filtered through a 40-μm cell strainer to get single cells. For electroporation, 1 million h-iPSCs were resuspended in 100-μl buffer mixed with 2-μg PB-EF1A-GFP-puro plasmid (VectorBuilder) and 1-μg transposase plasmid (VectorBuilder). The electroporated cells were then plated on a 35-mm Matrigel-coated dish in mTeSR1 medium with 10 μM Y27632 (Selleckchem, catalog no. S1049). After 48 hours, culture medium was replaced by mTeSR1 medium with puromycin (10 μg/ml; Sigma-Aldrich, catalog no. P8833) and changed daily for 3 to 4 days.

modRNA synthesis and formulation

Chemically modRNA encoding ETV2 [modRNA(ETV2)] was generated by TriLink BioTechnologies LLC. In brief, modRNA(ETV2) was synthesized in vitro by T7 RNA polymerase–mediated transcription from a linearized DNA template, which incorporates the 5′ and 3′ untranslated regions (UTRs) and a poly-A tail. Specifically, ETV2, transcript variant 1 (NM_014209.3;ORF:ATGGACCTGTGGAACTGGGATGAGGCATCCCCACAGGAAGTGCCTCCAGGGAACAAGCTGGCAGGGCTTGAAGGAGCCAAATTAGGCTTCTGTTTCCCTGATCTGGCACTCCAAGGGGACACGCCGACAGCGACAGCAGAGACATGCTGGAAAGGTACAAGCTCATCCCTGGCAAGCTTCCCACAGCTGGACTGGGGCTCCGCGTTACTGCACCCAGAAGTTCCATGGGGGGCGGAGCCCGACTCTCAGGCTCTTCCGTGGTCCGGGGACTGGACAGACATGGCGTGCACAGCCTGGGACTCTTGGAGCGGCGCCTCGCAGACCCTGGGCCCCGCCCCTCTCGGCCCGGGCCCCATCCCCGCCGCCGGCTCCGAAGGCGCCGCGGGCCAGAACTGCGTCCCCGTGGCGGGAGAGGCCACCTCGTGGTCGCGCGCCCAGGCCGCCGGGAGCAACACCAGCTGGGACTGTTCTGTGGGGCCCGACGGCGATACCTACTGGGGCAGTGGCCTGGGCGGGGAGCCGCGCACGGACTGTACCATTTCGTGGGGCGGGCCCGCGGGCCCGGACTGTACCACCTCCTGGAACCCGGGGCTGCATGCGGGTGGCACCACCTCTTTGAAGCGGTACCAGAGCTCAGCTCTCACCGTTTGCTCCGAACCGAGCCCGCAGTCGGACCGTGCCAGTTTGGCTCGATGCCCCAAAACTAACCACCGAGGTCCCATTCAGCTGTGGCAGTTCCTCCTGGAGCTGCTCCACGACGGGGCGCGTAGCAGCTGCATCCGTTGGACTGGCAACAGCCGCGAGTTCCAGCTGTGCGACCCCAAAGAGGTGGCTCGGCTGTGGGGCGAGCGCAAGAGAAAGCCGGGCATGAATTACGAGAAGCTGAGCCGGGGCCTTCGCTACTACTATCGCCGCGACATCGTGCGCAAGAGCGGGGGGCGAAAGTACACGTACCGCTTCGGGGGCCGCGTGCCCAGCCTAGCCTATCCGGACTGTGCGGGAGGCGGACGGGGAGCAGAGACACAATAA; 1029 bp) was cloned into the mRNA expression vector pmRNA, which contains a T7 RNA polymerase promoter, an unstructured synthetic 5′UTR, a multiple cloning site, and a 3′UTR that was derived from the mouse ⟨-globin 3′ gene. In vitro transcriptional reaction (1-ml scale) was performed to generate unmodified mRNA transcripts with wild-type bases and a poly-A tail. Cotranscriptional capping with CleanCap Cap1 AG trimer yields a naturally occurring Cap1 structure. Deoxyribonuclease treatment was used to remove DNA template. 5′-Triphosphate

was removed by phosphatase treatment to reduce innate immune response. After elution through a silica membrane, the purified RNA was dissolved in ribonuclease-free sodium citrate buffer (1 mM, pH 6.4).

Differentiation of h-iPSCs into h-iECs

S1-modETV2 protocol (4 days)

h-iPSCs were dissociated into single cells with TrypLE Select (Thermo Fisher Scientific, catalog no. 12563-029) and plated on Matrigel at a density of 50,000 cells/cm^2 in mTeSR1 medium with 10 μM Y27632. After 24 hours, the medium was changed to S1 medium consisting of basal medium supplemented with 6 μM CHIR99021 (Sigma-Aldrich, catalog no. SML1046). Basal medium was prepared by adding 1× GlutaMax supplement (Thermo Fisher Scientific, catalog no. 35050061) and L-Ascorbic acid (60 μg/ml; Sigma-Aldrich, catalog no. A8960) into Advanced Dulbecco's modified Eagle's medium (DMEM)/F12 (Thermo Fisher Scientific, catalog no. 12634010). After 48 hours, h-MPCs were dissociated into single cells and then transfected with modRNA(ETV2) by either electroporation or lipofection. For electroporation, 2 million h-MPCs were resuspended in 100-μl buffer mixed with 1-μg modETV2. Electroporated cells were then seeded on a 60-mm Matrigel-coated dish in modETV2 medium consisting of basal medium supplemented with VEGF-A (50 ng/ml; PeproTech, catalog no. 100-20), fibroblast growth factor 2 (FGF-2; 50 ng/ml; PeproTech, catalog no. 100-18B), EGF (10 ng/ml; PeproTech, catalog no. AF-100-15), and 10 μM SB431542 (Selleckchem, catalog no. S1067). For lipofection, 3 μl of Lipofectamine RNAiMax (Thermo Fisher Scientific, catalog no. 13778030) was diluted in 50 μl of Opti-MEM (Thermo Fisher Scientific, catalog no. 31985062) and 0.6 μg of modRNA(ETV2) diluted in another 50 μl of Opti-MEM. Lipofectamine and modRNA(ETV2) were then mixed and incubated for 15 min at RT. The lipid/RNA complex was added to 0.5 million h-MPCs in modETV2 medium, and transfected cells were then seeded on a 35-mm Matrigel-coated dish. Upon transfection (electroporation or lipofection), cells were cultured for another 48 hours before purification. Medium was changed every day throughout this protocol. modRNA encoding GFP (TriLink, catalog no. L-7601) at a concentration of 0.2 μg per million h-MPCs served as negative control.

Early modETV2 protocol (2 days)

h-iPSCs were dissociated into single cells and then transfected with modRNA(ETV2) by electroporation. For electroporation, 2 million h-iPSCs were resuspended in 100-μl buffer and mixed with 1.5-μg modRNA(ETV2). Electroporated cells were then plated on a 60-mm Matrigel-coated dish in mTeSR1 medium with 10 μM Y27632. After 24 hours, the medium was changed to mTeSR1 medium with 10 μM SB431542 for another 24 hours.

S1-S2, method no.1 (4 days)

h-iPSCs were dissociated into single cells with TrypLE Select and plated on Matrigel at a density of 50,000 cells/cm^2 in mTeSR1 medium with 10 μM Y27632. After 24 hours, the medium was changed to S1 medium consisting of basal medium supplemented with 6 μM CHIR99021. Basal medium was prepared by adding 1× GlutaMax supplement and L-Ascorbic acid (60 μg/ml) into Advanced DMEM/F12. After 48 hours, the differentiation medium was changed to S2 medium for 48 hours. S2 medium consisted of basal medium supplemented with VEGF-A (50 ng/ml), FGF-2 (50 ng/ml), EGF (10 ng/ml), and 10 μM SB431542. (Please note that all basal medium and supplement concentrations were identical to those used in the S1-modETV2 method.) Medium was changed every day throughout this protocol.

S1-S2, method no. 2 (8 days)

h-iPSCs were dissociated into single cells with TrypLE Select and plated on Matrigel at a density of 60,000 cells/cm^2 in mTeSR1 medium with 10 μM Y27632. After 24 hours, the medium was changed to STEMdiff APEL2 medium (STEMCELL Technologies, catalog no. 05275) supplemented with 6 μM CHIR99021. After 48 hours, the differentiation medium was changed to S2 medium for 48 hours. S2 medium consisted of STEMdiff APEL2 medium supplemented with VEGF-A (50 ng/ml), FGF-2 (10 ng/ml), and BMP4 (25 ng/ml) (PeproTech, catalog no. 120-05ET). Medium was changed every day throughout the first 4 days. Cells were lifted at day 4 and seeded on a p100 dish at 50,000 cells/cm^2 in EGM-2 with additional VEGF (50 ng/ml) for another 4 days. This protocol is adapted from Harding *et al.* (*18*).

S1-S2, method no. 3 (5 days)

h-iPSCs were dissociated into single cells with TrypLE Select and plated on Matrigel at a density of 50,000 cells/cm^2 in mTeSR1 medium with 10 μM Y27632. After 24 hours, the medium was changed to basal medium supplemented with 1 μM CP21R7 (Selleckchem, catalog no. S7954) and BMP4 (20 ng/ml). Basal medium was prepared by adding 1× B27 supplement (Thermo Fisher Scientific, catalog no. 17504044) and 1× N2 (Thermo Fisher Scientific, catalog no. 17502048) into DMEM/F12 (Thermo Fisher Scientific, catalog no. 11330032). After 72 hours, the differentiation medium was changed to S2 medium for 48 hours. S2 medium consisted of StemPro-34 SFM (Thermo Fisher Scientific, catalog no. 10639011) supplemented with VEGF-A (50 ng/ml), and 10 μM DAPT (Selleckchem, catalog no. S2215). Medium was changed every day throughout this protocol. This protocol is adapted from Sahara *et al.* (*19*).

S1-S2, method no. 4 (5 days)

h-iPSCs were dissociated into single cells with TrypLE Select and plated on Matrigel at a density of 50,000 cells/cm^2 in mTeSR1 medium with 10 μM Y27632. After 24 hours, the medium was changed to basal medium supplemented with 8 μM CHIR99021. Basal medium was prepared by adding 1× B27 supplement and 1× N2 into DMEM/F12. After 72 hours, the differentiation medium was changed to S2 medium for 48 hours. S2 medium consisted of StemPro-34 SFM supplemented with 200 ng/ml VEGF-A and 2 μM forskolin (Sigma-Aldrich, catalog no. F3917). Medium was changed every day throughout this protocol. This protocol is adapted from Patsch *et al.* (*4*).

Purification and expansion of h-iECs

At indicated time points after differentiation, h-iECs were dissociated into single cells and sorted into CD31$^+$ and CD31$^-$ cells using magnetic beads coated with anti-human CD31 antibodies (DynaBeads, Thermo Fisher Scientific, catalog no. 11155D). The purified CD31$^+$ h-iECs were then expanded in culture on 10-cm dishes coated with 1% gelatin. Culture medium for h-iECs was prepared by adding Endothelial Cell Growth medium 2 kit supplements into basal medium (except for hydrocortisone; PromoCell, catalog no. C22111) with 1× GlutaMax supplement and 10 μM SB431542.

RNA-seq analysis

The following groups were analyzed: h-iPSCs, human ECFCs, and h-iECs generated with three protocols: S1-S2, S1-modETV2, and early modETV2. Each group consists of three biological replicates. Total RNA from h-iECs that have been expanded for 7 days was extracted using RNeasy Mini Kit (Qiagen) following the manufacturer's protocol. RNA quantity and quality were checked with NanoDrop and Agilent Bioanalyzer instruments. Libraries were prepared and sequenced by

Genewiz (NJ, USA). Library preparation involved mRNA enrichment and fragmentation, chemical fragmentation, first- and second-strand complementary DNA (cDNA) synthesis, end repair and 5′ phosphorylation, dA-tailing, adaptor ligation, and PCR enrichment. The libraries were then sequenced using the Illumina HiSeq 2500 platform (Illumina, CA) using 2 × 150 paired-end configuration. The raw sequencing data (FASTQ files) were examined for library generation and sequencing quality using FastQC (www.bioinformatics.babraham.ac.uk/projects/fastqc/) to ensure that data quality was suitable for further analysis. Reads were aligned to UCSC (University of California, Santa Cruz) hg38 genome using the STAR aligner (*36*). Alignments were checked for evenness of coverage, rRNA content, genomic context of alignments, complexity, and other quality checks using a combination of FastQC, Qualimap (*37*), and MultiQC (*38*). The expression of the transcripts was quantified against the Ensembl release GRCh38 transcriptome annotation using Salmon. These transcript abundances were then imported into R (version 3.5.1) and aggregated to the gene level with tximport. Differential expression at the gene level was called with DESeq2 (*39*). Pairwise differential expression analysis between groups was performed using Wald significance test. The *P* values were corrected for multiple hypothesis testing with the Benjamini-Hochberg false discovery rate procedure (adjusted *P* value). Genes with adjusted $P < 0.05$ were considered significantly different. Hierarchical clustering and principal components analysis were performed on DESeq2-normalized, rlog variance–stabilized reads. All samples comparison was performed using likelihood ratio test. Heat maps of the differential expressed genes and enriched gene sets were generated with pheatmap package. Functional enrichment of differential expressed genes, using gene sets from GO, was determined with Fisher's exact test as implemented in the clusterProfiler package. The RNA-seq datasets are deposited online with SRA (Sequence Read Archive) accession no.: PRJNA509218.

Flow cytometry

Cells were dissociated into single-cell suspensions using TrypLE and washed with phosphate-buffered saline (PBS) supplemented with 1% bovine serum albumin and 0.2 mM EDTA. In indicated experiments, cells were stained with flow cytometry antibodies and analyzed using a Guava easyCyte 6HT/2 L flow cytometer (Millipore Corporation, Billerica, MA) and FlowJo software (Tree Star Inc., Ashland, OR). Antibody labeling was carried out for 10 min on ice followed by three washes with PBS buffer. Antibody information is detailed in table S1.

Microscopy

Images were taken using an Axio Observer Z1 inverted microscope (Carl Zeiss) and AxioVision Rel. 4.8 software. Fluorescent images were taken with an ApoTome.2 Optical sectioning system (Carl Zeiss) and 20× objective lens. Nonfluorescent images were taken with an AxioCam MRc5 camera using a 5× or 10× objective lens.

Immunofluorescence staining

Cells were seeded in eight-well LAB-TEK chamber slides at a density of 60,000 cells/cm^2. After confluency, cells were fixed in 4% paraformaldehyde (PFA), permeabilized with 0.1% Triton X-100 in PBS, and then blocked for 30 min in 5% horse serum (Vector Laboratories, catalog no. S-2000). Subsequently, cells were incubated with primary antibodies for 30 min at RT. Cells were washed three times with PBS and then incubated with secondary antibodies for 30 min at RT. Cells were washed three times with PBS and stained with 4′,6-diamidino-2-phenylindole (DAPI; 0.5 μg/ml) for 5 min. Slides were mounted with DAKO fluorescence mounting medium (Agilent, catalog no. S302380-2). Antibody information is detailed in table S1.

Spheroid sprouting assay

EC spheroids were generated by carefully depositing 500 h-MSCs and 500 h-iECs-GFP in 20-μl spheroid-forming medium on the inner side of a 10-cm dish lid. The spheroid-forming medium contained 0.24% (w/v) methyl cellulose (Sigma, catalog no. M0512). The lid was then turned upside down and placed on top of the plate filled with 10-ml sterile water. EC spheroids were collected after 2 days in culture and embedded in fibrin gel prepared with fibrinogen (5 mg/ml; Sigma-Aldrich, catalog no. F8630) and thrombin (0.5 U/ml; Sigma, catalog no. T-9549). A 100-μl fibrin gel/spheroid solution was spotted into the center of a 35-mm glass-bottom dish (MatTek, catalog no. P35G-1.5-10-C) and incubated for 10 min at 37°C for solidification. Gel/spheroid constructs were kept in culture for 3 days. GFP$^+$ sprouts were imaged using an inverted fluorescence microscope, and sprout lengths were measured by ImageJ.

Shear stress response assay

Confluent monolayers of h-iECs in a 100-mm culture dish were subjected to orbital shear stress for 24 hours at a rotating frequency of 150 rpm using an orbital shaker (VWR, Model 1000) positioned inside a cell culture incubator. After 24 hours, cells were fixed in 4% PFA and stained using an anti-human VE-Cadherin antibody. Alignment of ECs was visualized using an inverted fluorescence microscope under a 10× objective. Only the cells in the periphery of the culture dish were imaged. Cell orientation angles were measured by ImageJ.

NO production assay

Cells were cultured on gelatin-coated 12-well plates (2×10^5 cells per well) in h-iEC media. To measure NO, media were changed to fresh media containing 1 μM 4-amino-5-methylamino-2′,7′-difluorofluorescein diacetate (DAF-FM; Cayman, catalog no. 18767). Cells were cultured for 30 min and then harvested for flow cytometric analysis and fluorescent imaging. To suppress NO production, h-iECs were cultured in the presence of 5 mM L-NAME (Cayman Chemical, catalog no. 80210) for 24 hours. DAF-FM is nonfluorescent until it reacts with NO to form a fluorescent benzotriazole (fluoroscein isothiocyanate channel). The mean fluorescence intensities were measured by calculating the geometric mean in FlowJo.

Leukocyte adhesion molecules and leukocyte adhesion assays

Cells were cultured on a gelatin-coated 48-well plate (10^5 cells per well) in h-iEC medium. At confluency, cells were treated with or without TNF-α (10 ng/ml; PeproTech, catalog no. 300-01A) for 5 hours. Cells were then lifted and treated with anti–ICAM-1, anti–E-selectin, or anti–VCAM-1 antibodies for flow cytometry. For leukocyte adhesion assay, human HL-60 leukocytes were used. HL-60 cells were culture in leukocyte medium consisting of RPMI 1640 (Thermo Fisher Scientific, catalog no. 11875093) supplemented with 20% FBS. HL-60 cells (2×10^5) were suspended in 0.2-ml fresh leukocyte medium and added to each well. After gentle shaking for 45 min in cold room, plates were gently washed twice with cold leukocyte media. Cells were fixed in 2.5% (v/v) glutaraldehyde at RT for 30 min and then imaged. Bound leukocytes were quantified by ImageJ analysis software.

Smooth muscle cell differentiation assay

h-MSCs (2×10^4) and h-iECs (5×10^4) were plated in one well of an eight-well LAB-TEK chamber slide coated by 1% gelatin and cultured in h-iEC medium without SB431542 for 7 days. Smooth muscle cell–positive cells were stained with an anti–smooth muscle myosin heavy chain 11 antibody, and ECs and nucleus were stained by anti-VECAD (vasculate endothelial cadherin) antibody and DAPI, respectively. h-MSCs that were transduced with lentivirus to express GFP (h-MSCs-GFP) were used in indicated experiments. Antibody information is detailed in table S1.

Tube formation assay

h-iECs (8×10^3) were plated in one well of a 96-well plate on top of solidified Matrigel (50 μl) with h-iEC media. After 6 hours, cells were incubated with 1 μM Calcein-AM (BioLegend, catalog no. 425201) for 10 min and then imaged using a fluorescence microscope. Numbers of branches were counted by ImageJ.

In vivo vascular network–forming assay

Six-week-old NOD-SCID mice were purchased from the Jackson laboratory (Boston, MA). Mice were housed in compliance with Boston Children's Hospital guidelines, and all animal-related protocols were approved by the Institutional Animal Care and Use Committee. h-iECs for implantation were expanded for 7 days in vitro after differentiation unless otherwise specified. h-iECs were pretreated with 20 μM caspase inhibitor/Z-VAD-FMK (APExBio, catalog no. A1902) and 0.5 μM BCL-XL-BH4 (Millipore, catalog no. 197217) in h-iEC medium overnight before implantation. Briefly, h-iECs and h-MSCs (2×10^6 total per mouse, 1:1 ratio) or h-iECs alone (1×10^6 cells per mouse) were resuspended in 200 μl of pH-neutral pregel solution containing bovine collagen I (3 mg/ml; Trevigen, catalog no. 3442-050-01), fibrinogen (3 mg/ml), 50 μl of Matrigel (Corning, catalog no. 354234), FGF-2 (1 μg/ml; PeproTech, catalog no. 100-18B), and erythropoietin (1 μg/ml; ProSpec, catalog no. CYT-201). During anesthesia, mice were first injected with 50 μl of thrombin (10 U/ml; Sigma-Aldrich, catalog no. T4648) subcutaneously and then injected with 200 μl of cell-laden pregel solution into the same site. All experiments were carried out in five mice, and explants were harvested after 1 week and 1 month.

Histology and immunofluorescence staining

Explanted grafts were fixed overnight in 10% buffered formalin, embedded in paraffin, and sectioned (7 μm thick). Microvessel density was reported as the average number of erythrocyte-filled vessels (vessels/mm^2) in H&E-stained sections from the middle of the implants. For immunostaining, sections were deparaffinized, and antigen retrieval was carried out with boiling citric buffer (10 mM sodium citrate, 0.05% Tween 20, pH 6.0) for 30 min. Proteinase K (Abcam, catalog no. ab64220) treatment for 15 min was only applied to retrieve the mouse-specific CD31. Sections were then blocked for 30 min in 5% horse serum and incubated with primary and secondary antibodies for 30 min at RT. Fluorescent staining was performed using fluorescently conjugated secondary antibodies followed by DAPI counterstaining. Human-specific anti-CD31 antibody and UEA-1 lectin were used to stain human blood vessels. Perivascular cells were stained by anti–α-SMA antibody. Primary and secondary antibodies are detailed in table S1. The Click-It Plus TUNEL assay (Thermo Fisher Scientific, catalog no. C10617) was used to detect apoptotic cells in tissue.

Perfusion of human vessels

To test for perfusion of the human vessels, 1 week after h-iECs were implanted, biotinylated UEA-I (50 μg per mouse) was injected through the retro-orbital sinus. Thirty minutes after injection, mice were euthanized, and the implants were harvested. Perfused human vessels were identified as lumens with bound biotinylated UEA-I. Streptavidin Texas Red was applied to the histological sections of the grafts to visualize UEA-1$^+$ vessels. Sections were also stained with human-specific anti-CD31 to confirm the presence of human ECs.

Western blot

Cells were lysed with RIPA Lysis Buffer (Thermo Fisher Scientific, catalog no. 89901) in the presence of protease inhibitor. The concentration of extracted protein was measured using Pierce 660 nm Protein Assay Reagent (Thermo Fisher Scientific, catalog no. 1861426) and the Bio-Rad SmartSpec 3000 spectrophotometer. Forty micrograms of whole-cell protein lysate was applied to 4 to 15% Mini-PROTEAN TGX precast protein gel (Bio-Rad, catalog no. 4561084) with electrophoresis and then transferred to a nitrocellulose membrane. The probed primary antibodies were detected by using horseradish peroxidase–conjugated secondary antibodies and the Enhanced Chemiluminescent detection system (GE Health, catalog no. 28906836). Primary and secondary antibodies are detailed in table S1.

Quantitative reverse transcription PCR

Quantitative reverse transcription PCR was carried out in RNA lysates prepared from cells in culture. Total RNA was isolated with an RNeasy kit (Qiagen, catalog no. 74106), and cDNA was prepared using reverse transcriptase III (Thermo Fisher Scientific, catalog no. 4368814), according to the manufacturer's instructions. Quantitative PCR was performed using SRBR Green Master Mix (Thermo Fisher Scientific, catalog no. A25776), and detection was achieved using the StepOnePlus Real-time PCR system thermocycler (Applied Biosystems). Expression of target genes was normalized to glyceraldehyde-3-phosphate dehydrogenase (GAPDH). Real-time PCR primer sequences are listed in table S2.

Statistical analyses

Unless otherwise stated, data were expressed as means ± SD of the mean. For comparisons between two groups, means were compared using unpaired two-tailed Student's t tests. Comparisons between multiple groups were performed by analysis of variance (ANOVA) followed by Bonferroni's posttest analysis. Samples size, including number of mice per group, was chosen to ensure adequate power and were based on historical data. No exclusion criteria were applied for all analyses. All statistical analyses were performed using GraphPad Prism v.5 software (GraphPad Software Inc.). $P < 0.05$ was considered statistically significant.

SUPPLEMENTARY MATERIALS

Supplementary material for this article is available at http://advances.sciencemag.org/cgi/content/full/6/30/eaba7606/DC1

View/request a protocol for this paper from *Bio-protocol*.

REFERENCES AND NOTES

1. W. C. Aird, Endothelium in health and disease. *Pharmacol. Rep.* **60**, 139–143 (2008).
2. B.-S. Ding, D. J. Nolan, P. Guo, A. O. Babazadeh, Z. Cao, Z. Rosenwaks, R. G. Crystal, M. Simons, T. N. Sato, S. Worgall, K. Shido, S. Y. Rabbany, S. Rafii, Endothelial-derived

angiocrine signals induce and sustain regenerative lung alveolarization. *Cell* **147**, 539–553 (2011).
3. D. T. Paik, L. Tian, J. Lee, N. Sayed, I. Y. Chen, S. Rhee, J.-W. Rhee, Y. Kim, R. C. Wirka, J. W. Buikema, S. M. Wu, K. Red-Horse, T. Quertermous, J. C. Wu, Large-scale single-cell RNA-seq reveals molecular signatures of heterogeneous populations of human induced pluripotent stem cell-derived endothelial cells. *Circ. Res.* **123**, 443–450 (2018).
4. C. Patsch, L. Challet-Meylan, E. C. Thoma, E. Urich, T. Heckel, J. F. O'Sullivan, S. J. Grainger, F. G. Kapp, L. Sun, K. Christensen, Y. Xia, M. H. C. Florido, W. He, W. Pan, M. Prummer, C. R. Warren, R. Jakob-Roetne, U. Certa, R. Jagasia, P.-O. Freskgård, I. Adatto, D. Kling, P. Huang, L. I. Zon, E. L. Chaikof, R. E. Gerszten, M. Graf, R. Iacone, C. A. Cowan, Generation of vascular endothelial and smooth muscle cells from human pluripotent stem cells. *Nat. Cell Biol.* **17**, 994–1003 (2015).
5. S. Hu, M.-T. Zhao, F. Jahanbani, N.-Y. Shao, W. H. Lee, H. Chen, M. P. Snyder, J. C. Wu, Effects of cellular origin on differentiation of human induced pluripotent stem cell–derived endothelial cells. *JCI Insight* **1**, e85558 (2016).
6. H. Kataoka, M. Hayashi, R. Nakagawa, Y. Tanaka, N. Izumi, S. Nishikawa, M. L. Jakt, H. Tarui, S.-I. Nishikawa, Etv2/ER71 induces vascular mesoderm from Flk1^{+}PDGFRα^{+} primitive mesoderm. *Blood* **118**, 6975–6986 (2011).
7. S.-Y. Oh, J. Y. Kim, C. Park, The ETS factor, ETV2: A master regulator for vascular endothelial cell development. *Mol. Cells* **38**, 1029–1036 (2015).
8. A. Ferdous, A. Caprioli, M. Iacovino, C. M. Martin, J. Morris, J. A. Richardson, S. Latif, R. E. Hammer, R. P. Harvey, E. N. Olson, M. Kyba, D. J. Garry, Nkx2–5 transactivates the *Ets-related protein 71* gene and specifies an endothelial/endocardial fate in the developing embryo. *Proc. Natl. Acad. Sci. U.S.A.* **106**, 814–819 (2009).
9. D. Lee, C. Park, H. Lee, J. J. Lugus, S. H. Kim, E. Arentson, Y. S. Chung, G. Gomez, M. Kyba, S. Lin, R. Janknecht, D.-S. Lim, K. Choi, ER71 acts downstream of BMP, Notch, and Wnt signaling in blood and vessel progenitor specification. *Cell Stem Cell* **2**, 497–507 (2008).
10. R. Morita, M. Suzuki, H. Kasahara, N. Shimizu, T. Shichita, T. Sekiya, A. Kimura, K.-i. Sasaki, H. Yasukawa, A. Yoshimura, ETS transcription factor ETV2 directly converts human fibroblasts into functional endothelial cells. *Proc. Natl. Acad. Sci. U.S.A.* **112**, 160–165 (2015).
11. S. Lee, C. Park, J. W. Han, J. Y. Kim, K. Cho, E. J. Kim, S. Kim, S.-J. Lee, S. Y. Oh, Y. Tanaka, I.-H. Park, H. J. An, C. M. Shin, S. Sharma, Y.-s. Yoon, Direct reprogramming of human dermal fibroblasts into endothelial cells using ER71/ETV2. *Circ. Res.* **120**, 848–861 (2017).
12. G. Yan, R. Yan, C. Chen, C. Chen, Y. Zhao, W. Qin, M. B. Veldman, S. Li, S. Lin, Engineering vascularized skeletal muscle tissue with transcriptional factor ETV2-induced autologous endothelial cells. *Protein Cell* **122**, 3982–3222 (2018).
13. A. Le Bras, B. Yu, S. I. Bhaloo, X. Hong, Z. Zhang, Y. Hu, Q. Xu, Adventitial Sca1+ cells transduced with ETV2 are committed to the endothelial fate and improve vascular remodeling after injury. *Arterioscler. Thromb. Vasc. Biol.* **38**, 232–244 (2018).
14. I. Elcheva, V. Brok-Volchanskaya, A. Kumar, P. Liu, J.-H. Lee, L. Tong, M. Vodyanik, S. Swanson, R. Stewart, M. Kyba, E. Yakubov, J. Cooke, J. A. Thomson, I. Slukvin, Direct induction of haematoendothelial programs in human pluripotent stem cells by transcriptional regulators. *Nat. Commun.* **5**, 4372 (2014).
15. A. G. Lindgren, M. B. Veldman, S. Lin, ETV2 expression increases the efficiency of primitive endothelial cell derivation from human embryonic stem cells. *Cell Regen* **4**, 1 (2015).
16. K. Suknuntha, L. Tao, V. Brok-Volchanskaya, S. S. D'Souza, A. Kumar, I. Slukvin, Optimization of synthetic mRNA for highly efficient translation and its application in the generation of endothelial and hematopoietic cells from human and primate pluripotent stem cells. *Stem Cell Rev. Rep.* **14**, 525–534 (2018).
17. K. R. Chien, L. Zangi, K. O. Lui, Synthetic chemically modified mRNA (modRNA): Toward a new technology platform for cardiovascular biology and medicine. *Cold Spring Harb. Perspect. Med.* **5**, a014035 (2014).
18. A. Harding, E. Cortez-Toledo, N. L. Magner, J. R. Beegle, D. P. Coleal-Bergum, D. Hao, A. Wang, J. A. Nolta, P. Zhou, Highly efficient differentiation of endothelial cells from pluripotent stem cells requires the MAPK and the PI3K pathways. *Stem Cells* **35**, 909–919 (2017).
19. M. Sahara, E. M. Hansson, O. Wernet, K. O. Lui, D. Später, K. R. Chien, Manipulation of a VEGF-Notch signaling circuit drives formation of functional vascular endothelial progenitors from human pluripotent stem cells. *Cell Res.* **24**, 820–841 (2014).
20. T. L. Rasmussen, J. Kweon, M. A. Diekmann, F. Belema-Bedada, Q. Song, K. Bowlin, X. Shi, A. Ferdous, T. Li, M. Kyba, J. M. Metzger, N. Koyano-Nakagawa, D. J. Garry, ER71 directs mesodermal fate decisions during embryogenesis. *Development* **138**, 4801–4812 (2011).
21. T. L. Rasmussen, X. Shi, A. Wallis, J. Kweon, K. M. Zirbes, N. Koyano-Nakagawa, D. J. Garry, VEGF/Flk1 signaling cascade transactivates Etv2 gene expression. *PLOS ONE* **7**, e50103 (2012).
22. Y. Lin, C.-H. Gil, M. Yoder, Differentiation, evaluation, and application of human induced pluripotent stem cell–derived endothelial cells. *Arterioscler. Thromb. Vasc. Biol.* **37**, 2014–2025 (2017).
23. J. M. Melero-Martin, M. E. de Obaldia, S.-Y. Kang, Z. A. Khan, L. Yuan, P. Oettgen, J. Bischoff, Engineering robust and functional vascular networks in vivo with human adult and cord blood–derived progenitor cells. *Circ. Res.* **103**, 194–202 (2008).
24. A. N. Stratman, S. A. Pezoa, O. M. Farrelly, D. Castranova, L. E. Dye III, M. G. Butler, H. Sidik, W. S. Talbot, B. M. Weinstein, Interactions between mural cells and endothelial cells stabilize the developing zebrafish dorsal aorta. *Development* **144**, 115–127 (2017).
25. R.-Z. Lin, C. N. Lee, R. Moreno-Luna, J. Neumeyer, B. Piekarski, P. Zhou, M. A. Moses, M. Sachdev, W. T. Pu, S. Emani, J. M. Melero-Martin, Host non-inflammatory neutrophils mediate the engraftment of bioengineered vascular networks. *Nat. Biomed. Eng.* **1**, 0081 (2017).
26. K. Yamamizu, K. Kawasaki, S. Katayama, T. Watabe, J. K. Yamashita, Enhancement of vascular progenitor potential by protein kinase A through dual induction of Flk-1 and Neuropilin-1. *Blood* **114**, 3707–3716 (2009).
27. D. Klein, iPSCs-based generation of vascular cells: reprogramming approaches and applications. *Cell. Mol. Life Sci.* **75**, 1411–1433 (2018).
28. L. Yang, M. H. Soonpaa, E. D. Adler, T. K. Roepke, S. J. Kattman, M. Kennedy, E. Henckaerts, K. Bonham, G. W. Abbott, R. M. Linden, L. J. Field, G. M. Keller, Human cardiovascular progenitor cells develop from a KDR^{+} embryonic-stem-cell-derived population. *Nature* **453**, 524–528 (2008).
29. M. A. Vodyanik, J. Yu, X. Zhang, S. Tian, R. Stewart, J. A. Thomson, I. I. Slukvin, A mesoderm-derived precursor for mesenchymal stem and endothelial cells. *Cell Stem Cell* **7**, 718–729 (2010).
30. S. Casie Chetty, M. S. Rost, J. R. Enriquez, J. A. Schumacher, K. Baltrunaite, A. Rossi, D. Y. R. Stainier, S. Sumanas, Vegf signaling promotes vascular endothelial differentiation by modulating etv2 expression. *Dev. Biol.* **424**, 147–161 (2017).
31. Y. Chen, I. Amende, T. G. Hampton, Y. Yang, Q. Ke, J.-Y. Min, Y.-F. Xiao, J. P. Morgan, Vascular endothelial growth factor promotes cardiomyocyte differentiation of embryonic stem cells. *Am. J. Physiol. Heart Circ. Physiol.* **291**, H1653–H1658 (2006).
32. J. H. Lee, S. I. Protze, Z. Laksman, P. H. Backx, G. M. Keller, Human pluripotent stem cell-derived atrial and ventricular cardiomyocytes develop from distinct mesoderm populations. *Cell Stem Cell* **21**, 179–194.e4 (2017).
33. S. Han, A. Bourdon, W. Hamou, N. Dziedzic, O. Goldman, V. Gouon-Evans, Generation of functional hepatic cells from pluripotent stem cells. *J. Stem Cell Res. Ther.* **S10**, 1–7 (2012).
34. R.-Z. Lin, R. Moreno-Luna, D. Li, S.-C. Jaminet, A. K. Greene, J. M. Melero-Martin, Human endothelial colony-forming cells serve as trophic mediators for mesenchymal stem cell engraftment via paracrine signaling. *Proc. Natl. Acad. Sci. U.S.A.* **111**, 10137–10142 (2014).
35. J. M. Melero-Martin, Z. A. Khan, A. Picard, X. Wu, S. Paruchuri, J. Bischoff, In vivo vasculogenic potential of human blood-derived endothelial progenitor cells. *Blood* **109**, 4761–4768 (2007).
36. A. Dobin, C. A. Davis, F. Schlesinger, J. Drenkow, C. Zaleski, S. Jha, P. Batut, M. Chaisson, T. R. Gingeras, STAR: Ultrafast universal RNA-seq aligner. *Bioinformatics* **29**, 15–21 (2013).
37. F. García-Alcalde, K. Okonechnikov, J. Carbonell, L. M. Cruz, S. Götz, S. Tarazona, J. Dopazo, T. F. Meyer, A. Conesa, Qualimap: Evaluating next-generation sequencing alignment data. *Bioinformatics* **28**, 2678–2679 (2012).
38. P. Ewels, M. Magnusson, S. Lundin, M. Käller, MultiQC: Summarize analysis results for multiple tools and samples in a single report. *Bioinformatics* **32**, 3047–3048 (2016).
39. M. I. Love, W. Huber, S. Anders, Moderated estimation of fold change and dispersion for RNA-seq data with DESeq2. *Genome Biol.* **15**, 550 (2014).

Acknowledgments: Histology was supported by Core Facility of the Dana-Farber/Harvard Cancer Center (P30 CA06516). **Funding:** This work was supported by the National Institutes of Health (NIH; grants R01AR069038, R01HL128452, and R21AI123883 to J.M.M.-M.) and by the Juvenile Diabetes Research Foundation (JDRF; grant 3-SRA-2018-686-S-B to J.M.M.-M.). **Author contributions:** K.W., R.-Z.L., and J.M.M.-M. conceived and designed the project. K.W., R.-Z.L., A.H.N., X.H., C.N.L., J.N., G.W., X.W., and J.M.M.-M. performed the experimental work. All authors discussed and analyzed the data and edited the results. A.H.N., G.W., W.T.P., and G.M.C. provided crucial material. K.W. and J.M.M.-M. wrote the manuscript. **Competing interests:** G.M.C. and A.H.N. are cofounders of and have equity in GC Therapeutics Inc., which uses transcription factors for therapeutics. K.W., R.-Z.L., and J.M.M.-M. are inventors on a patent related to this work filed by the Children's Medical Center Corporation (no. 16/885,999, filed 28 May 2020). The authors declare no other competing interests. **Data and materials availability:** All data needed to evaluate the conclusions in the paper are present in the paper and/or the Supplementary Materials. Additional data related to this paper may be requested from the authors.

Submitted 2 January 2020
Accepted 9 June 2020
Published 24 July 2020
10.1126/sciadv.aba7606

Citation: K. Wang, R.-Z. Lin, X. Hong, A. H. Ng, C. N. Lee, J. Neumeyer, G. Wang, X. Wang, M. Ma, W. T. Pu, G. M. Church, J. M. Melero-Martin, Robust differentiation of human pluripotent stem cells into endothelial cells via temporal modulation of ETV2 with modified mRNA. *Sci. Adv.* **6**, eaba7606 (2020).